Neuroradiology (2013) 55:595–602
DOI 10.1007/s00234-013-1141-1

DIAGNOSTIC NEURORADIOLOGY

3D fat-saturated T1 SPACE sequence for the diagnosis of cervical artery dissection

Victor Cuvinciuc · Magalie Viallon · Isabelle Momjian-Mayor · Roman Sztajzel · Vitor Mendes Pereira · Karl-Olof Lovblad · Maria Isabel Vargas

Received: 6 December 2012 / Accepted: 14 January 2013 / Published online: 25 January 2013

Abstract
Introduction This study aims to demonstrate the added value of a 3D fat-saturated (FS) T1 sampling perfection with application-optimised contrast using different flip angle evolutions (SPACE) sequence compared to 2D FS T1 spin echo (SE) for the diagnosis of cervical artery dissection.
Methods Thirty-one patients were prospectively evaluated on a 1.5-T MR system for a clinical suspicion of acute or subacute cervical artery dissection with 3D T1 SPACE sequence. In 23 cases, the axial 2D FS T1 SE sequence was also used; only these cases were subsequently analysed. Two neuroradiologists independently and blindly assessed the 2D and 3D T1 sequences. The presence of recent dissection (defined as a T1 hyperintensity in the vessel wall) and the quality of fat suppression were assessed. The final diagnosis was established in consensus, after reviewing all the imaging and clinical data.
Results Overall sensitivity and specificity were 0.929 and 1 for axial T1 SE, and 0.965 and 0.945 for T1 SPACE ($P>0.05$), respectively. The two readers had excellent agreement for both sequences ($k=1$ and 0.8175 for T1 SE and T1 SPACE, respectively; $P>0.05$). The quality of the fat saturation was similar. Very good fat saturation was obtained in the upper neck. Multiplanar reconstructions were very useful in tortuous regions, such as the atlas loop of the vertebral artery or the carotid petrous entry. 3D T1 SPACE sequence has a shorter acquisition time (3 min 25 s versus 5 min 32 s for one T1 SE sequence) and a larger coverage area.
Conclusion 3D T1 SPACE sequence offers similar information with its 2D counterpart, in a shorter acquisition time and larger coverage area.

Keywords Cervical artery dissection · Magnetic resonance imaging · T1 fat-saturated · T1 SPACE sequence

V. Cuvinciuc · V. M. Pereira · K.-O. Lovblad · M. I. Vargas (✉)
Department of Diagnostic and Interventional Neuroradiology, DISIM,
University Hospitals of Geneva, Gabrielle-Perret-Gentil 4,
1205 Geneva, Switzerland
e-mail: maria.i.vargas@hcuge.ch

M. Viallon
Department of Radiology, DISIM, University Hospitals of Geneva, Geneva, Switzerland

I. Momjian-Mayor · R. Sztajzel
Department of Neurology, University Hospitals of Geneva, Geneva, Switzerland

Introduction

Cervical arterial dissection is a recognised cause of 10–25 % of the ischemic strokes in young and middle-aged patients [1]. Most commonly, the dissected arteries are the internal carotid (ICA) and vertebral arteries (VA); common carotid arteries are mostly involved in post-traumatic dissections or associated with aortic arch dissection [2]. Conventional angiography is considered the golden standard for dissection diagnosis due to the precise delineation of the luminal abnormalities, but its use is limited by its invasiveness and cost. Also, the failure to directly show the vessel wall hematoma is a serious limitation of this technique [3].

MR imaging has been described as a non-invasive method to diagnose dissection in a single comprehensive scan [4–8], showing both the luminal abnormalities and the vessel wall hematoma. Various techniques of MR angiography of the head and neck vessels, e.g. time of flight (TOF) or gadolinium-enhanced head and neck angiography, depict narrowing of the lumen or complete vessel occlusion. TOF sequence is sensitive to the moving protons and to the methemoglobin, having the potential of showing both the

circulating lumen and the wall hematoma [9], but it overestimates the high-grade stenosis and it is time consuming when used over large arterial segments, such as the whole length of the cervical arteries. Contrast-enhanced MR angiography has a short acquisition time and depicts well the permeable arterial lumen, but it is of limited value in showing the wall hematoma [8]. In doubtful cases, high-resolution MR sequences with surface coils could be also used [7, 10], but obtaining them in the acute phase might be difficult [9]. Currently, the diagnosis of the wall hematoma is based on 2D T1-weighted fat-saturated (FS) spin echo (SE) sequence [11]. Fat suppression imaging is required to clearly distinguish the hyperintensity associated with methemoglobin, suggestive of subacute intramural haemorrhage, from the surrounding fat tissue. Thin T1 SE FS axial slices need to be performed before contrast injection, hence, before the contrast-enhanced angiography can localise the suspected dissection, and so must cover all arteries of the neck. This becomes very time consuming when using an axial 2D sequence.

Sampling perfection with application-optimised contrast using different flip angle evolutions (SPACE) sequence with flexible reordering, optimised contrast and motion sensitising gradient can provide fast 3D isotropic T1 FS images, with very good dark blood contrast. They allow multiplanar and curved reconstruction that are of particular interest given the anatomical tortuosity of the carotid and vertebral arteries.

Our goal was to demonstrate that 3D T1 SPACE FS sequence could not only be a useful adjunct to a cervical artery dissection protocol but could also replace the FS T1 SE sequence.

Methods

Patients The study was approved by the local ethics committee. Thirty-one patients (18 men, 13 women) were included in this study. They all presented acutely with clinical symptoms suggestive of carotid or vertebral dissection (cervicalgia, headache, Horner syndrome and/or various central neurological deficits). Their mean age was 49.2±14.8 years. A neurologist experienced in the care of patients with cervical arteries dissection performed medical history and clinical examination.

MR acquisition All patients were examined on a 1.5-T Espree MRI scanner (Siemens, Erlangen, Germany). All scans were performed with the standard head and neck coil combination (18 elements). Twenty-three (74.2 %) of the patients had both axial T1 SE FS and 3D T1 SPACE FS sequences; only these patients were included in the subsequent analysis. All patients except patient number 6 had gadolinium-enhanced head and neck angiography.

To achieve long echo trains for the T1 SPACE sequence, the refocusing flip angles were adjusted to provide a specific prescribed signal evolution for T1 and T2 relaxation times of interest, with "target" T1 and T2 being new sequence parameters that can be set freely to control the flip angle variation [12]. In practice, it is not feasible to test several target T1, T2 pairs for contrast optimization of the 3D T1 weighted SPACE sequence for head and neck, and we fixed T1 target and T2 target values at 940 and 100 ms, respectively. Since view ordering can strongly influence image quality when signal modulation is present, the prototype 3D T1 SPACE sequence implements a new k-space reordering scheme that also improves flexibility and efficiency in setting acquisition parameters. For example, the turbo factor can now be accessed directly and echo train lengths can be controlled independently of matrix size [13]; it enables new parameters like elliptical scanning [14] and improves image quality by adapting the k-space sampling strategy to particular desired weighting and examinations environments. In our case, spatially selective excitation was used, followed by linearly reordered acquisition. A dummy echoes in the beginning of the echo train was also set.

Each 3D T1 SPACE FS acquisition consists of a large coronal stack with a left-right phase encoding direction and around 56 partitions. Fat saturation was obtained using a Spectral Adiabatic Inversion Recovery (SPAIR) fat saturation design. Parallel acquisition (iPAT=2) and variable flip angles along the echo train (T2 flip angle variation mode (evolution mode 1)) were used.

Axial T1 SE sequence was performed with the following parameters: echo time (TE) 10 ms, repetition time (TR) 817 ms, flip angle 150°, spectral saturation of fat, 2 excitations, field of view (FOV) 26×33 cm, 374×512 matrix, thickness 3 mm, 20 slices, and acquisition time 5 min 32 s. 3D T1 SPACE sequence was performed in coronal plane, with the following parameters: TE 22 ms, TR 750 ms, variable flip angle, SPAIR fat saturation mode, averages 1.4, FOV 23×23 cm, 256×256 matrix (interpolated 512×512), 56 slices, and acquisition time 3 min 25 s. Detailed MR parameters for 2D and 3D T1 FS sequences are given in Table 1.

Post-processing For each patient, coronal, oblique and/or curvilinear multiplanar reconstructions were generated from 3D T1 SPACE datasets. The 3D datasets were analysed using the 3D Syngo (Siemens, Erlangen Germany) task card. Thin maximum intensity projection or multiplanar reconstructions were obtained in any orientation depending on the region of interest.

Image evaluation Two image datasets containing the anonymised T1 SE FS and 3D T1 SPACE images for the 23 patients that had both sequences were retrospectively and independently evaluated by two neuroradiologists (V.C. and M.I.V. with 6 and 10 years of experience in neuroradiology, respectively), blinded to the final diagnosis. Dissection was

Table 1 Main parameters of the T1 SE FS and 3D T1 SPACE FS sequences

Sequence type	Number of slices/matrix	Voxel size (mm)	Flip angle (degrees)	TE (ms)/TR (ms)/TA (min)	Bandwidth (Hz/pixel)	Specific parameters
T1 SE FS	20/374×512	0.7×0.65×3	150°	10/817/5 min 32 s	215	Number of excitations=2, ETL=3, spectral saturation of fat, iPAT=2
3D T1 FS SPACE	56/256×256 (interpolated 512×512)	Isotropic 0.9 mm (interpolated isotropic 0.45 mm)	Variable	22/750/3 min 25 s	574	T1 flip angle var mode[a], averages=1.4, ETL =42, SPAIR fat saturation mode, iPAT=2, echo train duration=114, slab selective, partial Fourier allowed, 1 discarded echo, linear reordering

TE echo time, *TR* repetition time, *ETL* echo train length, *TA* acquisition time

[a] T1 var mode (TE=13 ms, TR=750 ms, TF=5, RF pulse type=normal, SPAIR fat sat)

diagnosed as a crescent T1 hyperintensity in the wall of carotid and/or vertebral arteries, with variable luminal abnormalities (from normal to occlusion). Each set of images was classified as "yes" or "no" for dissection. Additionally, they noted the quality of the fat saturation, according to the following scale: "diagnostic" (no fat visible in proximity of the vessels) and "non-diagnostic" (fat surrounding vessels not completely saturated).

Statistical analysis Interobserver agreement for each T1 FS sequence was estimated by using the kappa coefficient of agreement. Values were interpreted as suggested by Landis and Koch [15]. Two-tailed *t* test for independent samples with significance level of .05 was used.

Diagnosis The final diagnosis of acute dissection was established according to the clinical picture, physical examination, MR angiography signs of luminal abnormalities, and vessel wall hematoma on at least one T1 FS sequence [16]. When available, follow-up MR exams looking for modifications suggestive of previous dissection (normalisation of arterial lumen, disappearance of wall abnormalities, residual stenosis or occlusion, pseudo-aneurysm formation) were used to confirm the diagnosis.

Results

Final diagnosis of acute or subacute dissection was established in 14 patients (60.87 %). In one patient, we have found an old dissection, in another one, an acute atherosclerotic vertebral occlusion; the other seven patients (30.43 %) had no luminal or parietal arterial abnormalities. Follow-up MR imaging was available in 10 out of these 14 patients (71.43 %), showing three cases of normalisation of the vessel wall and lumen, two cases of residual stenosis, two cases of persistent occlusion and three cases of pseudo-aneurysmal formation.

Table 2 Clinical and imaging data of the patients with acute dissection

	Age/sex	Clinical picture	Mechanism	Artery involved	Ischemic lesion
1	61/M	Horner syndrome, hemiplegia	S	Left ICA	+
2	54/M	Hemiparesthesia, dysarthria	S	Right ICA	+
3	52/F	Horner syndrome	S	Right ICA	−
4	39/F	Right facial paralysis, dysarthria	S	Left ICA	+
5	36/M	Cerebellar syndrome	T	Left V2–V3	+
6	45/M	Horner syndrome, facial hypoesthesia	T	Left ICA	−
7	33/F	Cervicalgia	S	Left V2–V3	−
8	31/M	Horner syndrome, hemiparesthesia	T	Right V1–V2	−
9	49/M	Swallowing difficulties	S	Left V1–V2	+
10	61/M	Headache	S	Bilateral ICA	−
11	21/M	Coma	T	Right ICA	+
12	55/M	Visual troubles, Horner syndrome	S	Left ICA	−
13	44/M	Headache	S	Right V4	−
14	50/M	Aphasia, Horner syndrome	S	Left ICA	+

ICA internal carotid artery, *S* spontaneous, *T* traumatic

Main demographic and imaging data for the patients with acute dissection are provided in Table 2. Ages ranged between 21 and 61 years. These patients presented with various symptoms, including Horner syndrome, cervicalgia, headache, diverse motor and sensitive deficits and coma. The dissection was spontaneous in ten (71.43 %) of cases and traumatic in four (28.57 %) of cases.

MR examination was performed between 1 and 45 days after the symptom onset (mean interval 12±8 days).

Both T1 FS sequences showed similar T1 hyperintense patterns in the vessel wall, suggestive of recent hematoma (Figs. 1, 2, 3 and 4). No patient had the MR exam in the hyperacute phase (first 24 h after the onset). In three patients (1, 4 and 6), the MR exam was performed in the acute phase of evolution (between 1 and 3 days after the onset), and the wall hematoma was slightly T1 hyperintense, but clearly distinguishable as it was contrasted between the hypointense arterial flow and the saturated surrounding fat (Figs. 1 and 3). Patient 8 had the MR exam 45 days after the clinical onset, but the wall hematoma was still visible hyperintense on both T1 FS sequences. All the other patients were explored on MR in the subacute phase (between 3 and 30 days), with excellent visibility of the wall hematoma on both T1 sequences.

Sensitivity and specificity were not different for the two methods ($P>0.05$). Overall sensitivity and specificity were 0.929 and 1 for axial T1 SE FS, and 0.965 and 0.945 for T1

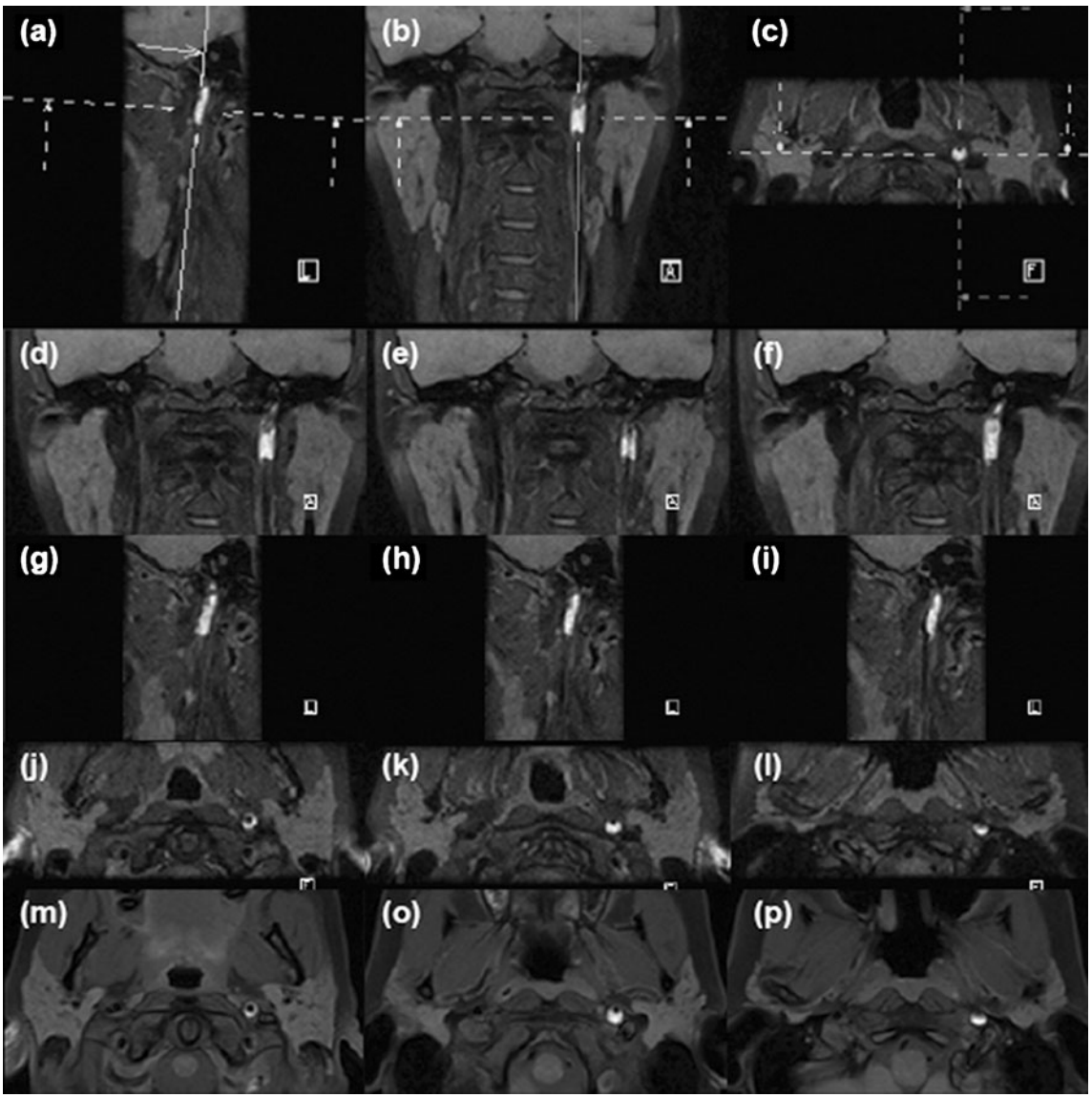

Fig. 1 Patient no. 4, 39-year-old woman, presented with right facial paralysis and dysarthria after coughing effort. Sagittal (**a**), coronal (**b**) and axial (**c**) reconstructions of 3D T1 FS SPACE images show the arterial wall hyperintensity in the pre-petrous segment of the left ICA. Contiguous thin MIP reconstructions clearly delineate the topography and the extension of the wall hematoma in the coronal (**d**–**f**), sagittal (**g**–**i**) and axial planes (**j**–**l**). Axial 2D T1 SE FS images (**m**–**p**) show the crescent-like hyperintensity of the wall hematoma

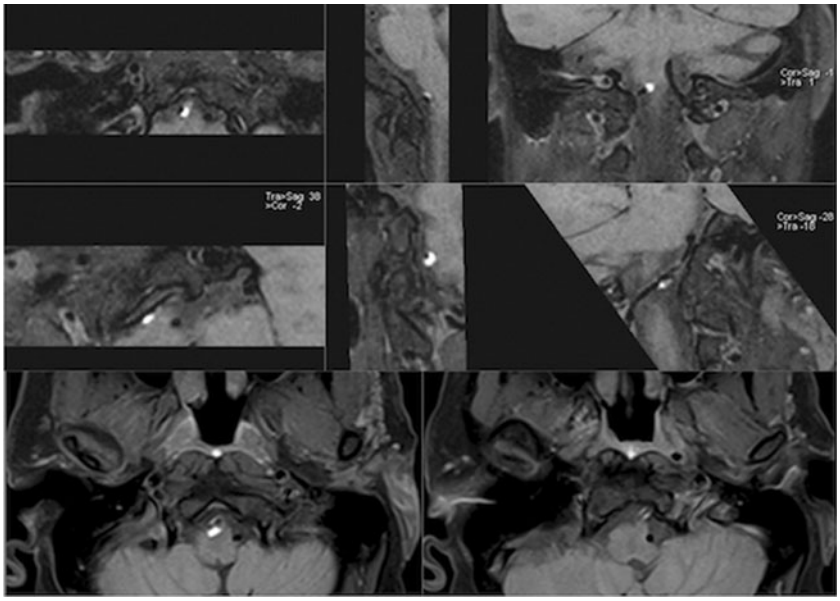

Fig. 2 Patient no. 13, 44-year-old male, presented with spontaneous headache. Multiple straight (*upper row*) and curvilinear (*middle row*) MPRs depict the topography and extension of the subacute mural hematoma in the V4 segment of the right vertebral artery. In the *lower row*, notice the corresponding axial images of the 2D T1 SE FS acquisition

SPACE, respectively. The two readers had very good agreement for both sequences (kappa=1 and 0.8175 for T1 SE and T1 SPACE, respectively; $P>0.05$).

The agreement between the two reviewers was excellent for the quality of fat saturation on T1 SE FS sequences; all cases were considered by both reviewers to have diagnostic fat saturation (no fat visible in proximity of the vessels). It is noteworthy that in 20 cases (86.95 %), the T1 SE FS sequence was performed only at the upper cervical level; in the remaining three cases, performed at the lower cervical level, the quality of fat saturation was considered appropriate by both reviewers, but there was always some remaining superficial fat hyperintense on T1.

On 3D FS T1 SPACE sequence, both reviewers considered 20 cases (86.96 %) to have diagnostic fat suppression included and one case to have non-diagnostic fat suppression (fat surrounding vessels at the lower cervical level not completely saturated). The remaining two cases involved disagreement over the quality of fat saturation in the lower cervical areas, surrounding the common carotid arteries and V1 segments of the vertebral arteries. The kappa coefficient of agreement between the two reviewers for diagnostic versus non-diagnostic categories was 0.465 (moderate agreement).

ICA was acutely dissected in nine patients (in five cases, the left ICA; three cases, right ICA; and in one case, both ICAs), always in the sub-petrous segment; in patient 14, there was an old dissection of the right ICA and a new dissection of the left ICA. We have found no case of common carotid artery dissection. VA was involved in five cases (left one in three cases and right one in two cases; V1–V2 in two cases, V2–V3 in two cases, only V4 in one case).

In six cases (42.86 %), cerebral ischemic lesions were found in the territory irrigated by the dissected artery.

Discussion

This study demonstrates the added value of the 3D T1 FS SPACE sequence, compared to the 2D T1 SE FS sequence, in patients with acute or subacute carotid or vertebral artery

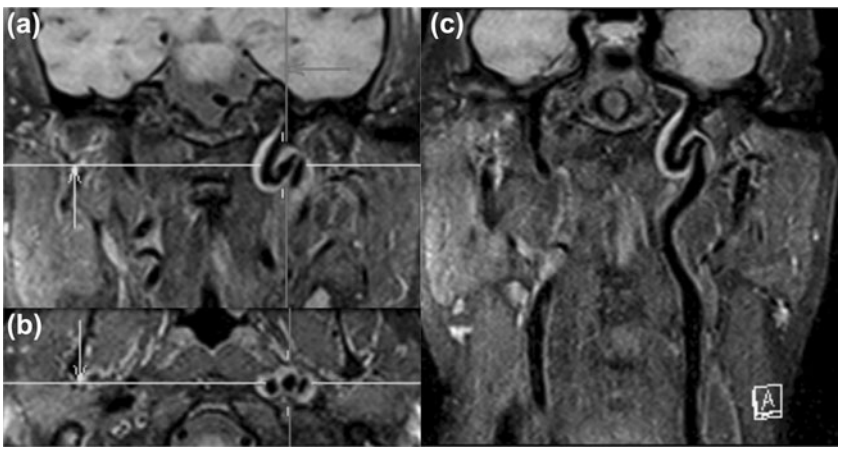

Fig. 3 Patient no. 1, 61-year-old man with Horner syndrome and right hemiplegia without any identified favouring factor. Coronal (**a**), axial (**b**) and curved (**c**) reconstructions of 3D T1 FS SPACE clearly delineate the wall hematoma's hyperintensity suggestive of subacute dissection of a very tortuous pre-petrous left ICA

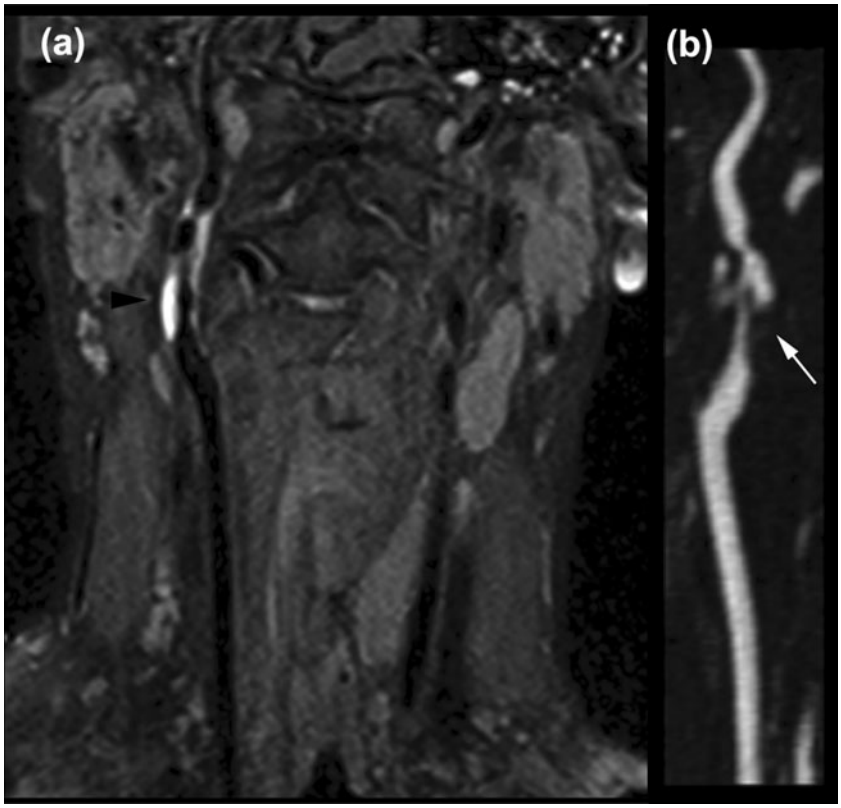

Fig. 4 Patient no. 2, 54-year-old man, presented with left hemiparesthesia and dysarthria after physical exercise. Coronal MIP reconstruction of 3D T1 FS SPACE (**a**) shows the subacute mural hematoma in the cervical right ICA (*black arrowhead*). MIP reconstruction of gadolinium-enhanced MR angiography of the head and neck vessels (**b**) shows a tapering stenosis of the ICA and two distal pseudo-aneurysms (*white arrow*)

dissection using a standard multi-array surface coil at 1.5 T. The advantages of the T1 3D FS SPACE sequence over 2D T1 FS sequence are multiple. First, a large and complete coverage of the head and neck area in one acquisition is possible. This feature appears to be very important as it may allow identifying and localising all lesions in a single acquisition. In order to have the same *z*-axis coverage, the axial T1 SE sequence should be performed twice, with a significant longer MR protocol. Second, 3D T1 FS SPACE sequence has a shorter acquisition time with the advantage of both shorter total MR protocol time and robustness to movement artefacts. 3D T1 SPACE sequence has an acquisition time of a little more than 3 min, compared to almost 11 min for two axial T1 sequences (necessary for covering the whole neck area). Third, it enables MPR parallel and curved reconstructions (Fig. 3) as well as thin maximum intensity projections (MIP) reconstruction. MIP reconstructions provide a panoramic view of the length of the hyperintense intramural hematoma, which is useful for correct localisation of the dissection, especially in tortuous arterial segments.

A direct comparison with 3D TOF sequence is beyond the scope of this article. Nonetheless, it seems that it has some advantages, or at least complementary information to TOF sequence, because it offers a natural "dark blood" contrast with very good visibility of the intramural hematoma, whereas on TOF ("white blood" sequence), the vessel wall hematoma can be distinguished from intraluminal flow signal only because of its relatively lower signal intensity and the separating intimal vessel boundary.

The intramural hematoma showed a wide variety of signal intensities from mild to moderate and very bright hyperintensities, depending on the age of the hematoma [17]. The T1 signal intensity was similar on the two FS sequences. Late controls showed the disappearance of the wall T1 hyperintensity (Fig. 5).

We have obtained a very good fat saturation in the head and neck area on T1 SPACE sequence in most patients. In the proximity of the shoulders, the superficial fat was suboptimally saturated, but the deep perivascular fat tissue was frequently properly saturated, allowing for identification of the V1 segment (Fig. 6). The two reviewers determined that the saturation of the fat surrounding the proximal cervical vessels was not satisfactory in only one case. In such cases, axial 2D T1 SE could be used as an alternative. In other segments of the vertebral arteries (such as V2 and V3), fat saturation was always excellent and subacute hematoma was clearly visible.

Patient 5 had been operated for a post-traumatic cervical disc hernia. We noticed relatively few artefacts on 3D T1 SPACE sequence related to the metallic surgical material, allowing for good visualisation of the adjacent vertebral arteries (Fig. 6). Post-operative metallic hardware is known to induce artefacts on T1 FS SE images, due to magnetic field (B0 and B1) inhomogeneity, rendering the analysis of the adjacent vertebral arteries extremely difficult [18].

We have also implemented this sequence for a 3-T Siemens Trio machine and it seems to offer similar advantages

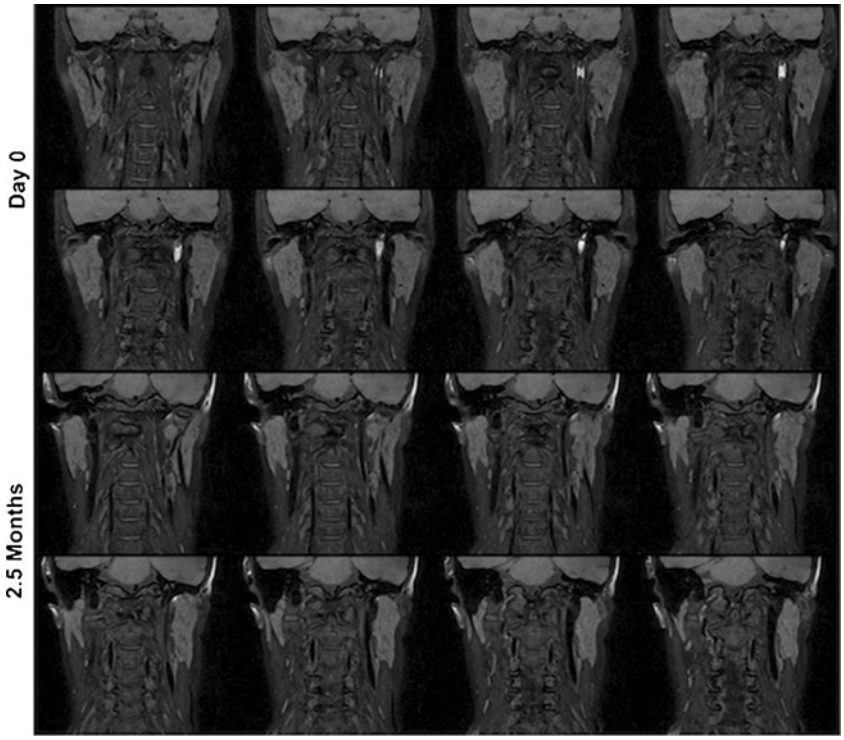

Fig. 5 Patient no. 4 (see above). Ten-week control shows complete disappearance of the arterial wall hyperintensity (*lower two rows*) compared to the acute phase (*upper two rows*)

compared to the axial T1 SE FS sequence. Similar approaches exist on other manufacturers of MR machines [19].

These initial results should be confirmed on larger series. The limitation of this sequence seems to be the incomplete saturation of fat in the lower cervical region, but usually the deep perivascular fat is properly saturated. The axial FS T1 SE sequence has also less than perfect fat saturation at the shoulders level, but it could be a useful alternative for the

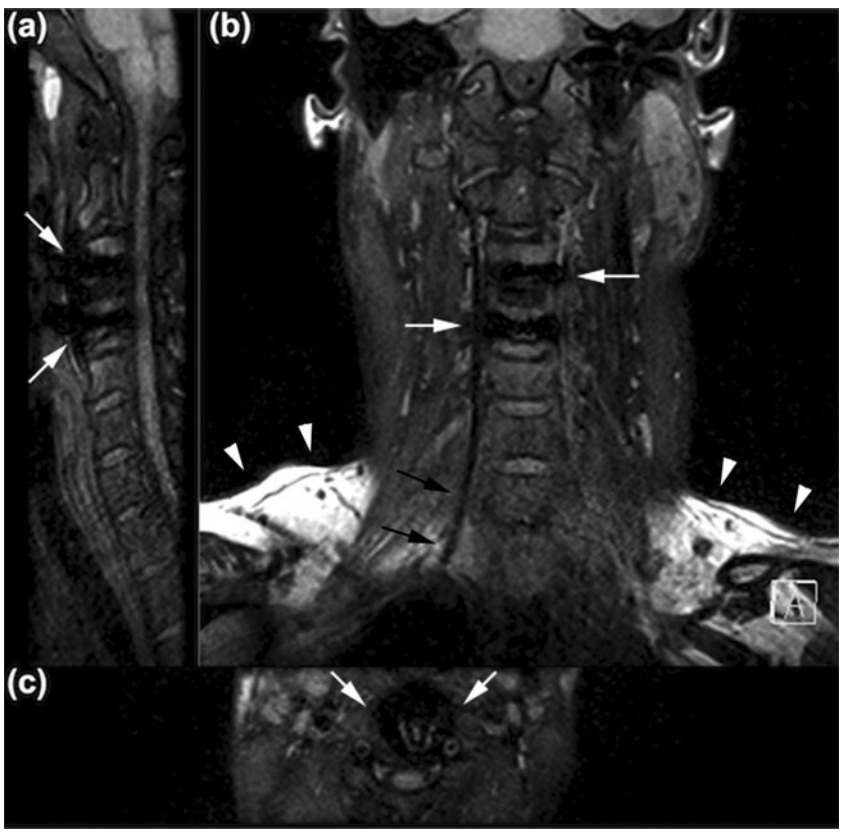

Fig. 6 Patient no. 5, 36-year-old male with C3–C4 disc hernia, adjacent spinal cord contusion and cerebellar syndrome after motor vehicle accident. Sagittal (**a**), coronal (**b**) and axial (**c**) MPRs show limited artefacts (*white arrows*) of the C3–C4 surgical material (metallic plate and interbody cage), with satisfactory visualisation of the vertebral arteries; the left vertebral artery was dissected at the V3–V4 levels (not shown). Note the suboptimal fat saturation in the subcutaneous fat planes at the level of the shoulders (*white arrowheads*), but proper saturation along the proximal vertebral arteries segments (*black arrows*)

analysis of the this region. We cannot exclude the possibility of false-negative results in our series on both T1 FS sequences, especially due to small vessel wall hematomas, but SPACE sequence seems to be better adapted to depict them, due to the superior spatial resolution.

Conclusion

3D T1 FS SPACE has the potential to replace the time consuming axial FS T1 SE sequence because it is a fast isotropic sequence offering a wide coverage of the neck, very good fat saturation and excellent delineation of wall hematoma in the acute and subacute phases of cervical arteries dissection.

Acknowledgments We thank Dominik Paul from Siemens Healthcare for his valuable support on the 3D FS T1 SPACE prototype sequence.

Conflict of interest We declare that we have no conflict of interest.

References

1. Ducrocq X, Lacour JC, Debouverie M, Bracard S, Girard F, Weber M (1999) Cerebral ischemic accidents in young subjects. A prospective study of 296 patients aged 16 to 45 years. Rev Neurol (Paris) 155(8):575–582
2. Zach V, Zhovtis S, Kirchoff-Torres KF, Weinberger JM (2012) Common carotid artery dissection: a case report and review of the literature. J Stroke Cerebrovasc Dis 21(1):52–60
3. Vertinsky AT, Schwartz NE, Fischbein NJ, Rosenberg J, Albers GW, Zaharchuk G (2008) Comparison of multidetector CT angiography and MR imaging of cervical artery dissection. AJNR Am J Neuroradiol 29(9):1753–1760
4. Brugieres P, Castrec-Carpo A, Heran F, Goujon C, Gaston A, Marsault C (1989) Magnetic resonance imaging in the exploration of dissection of the internal carotid artery. J Neuroradiol 16(1):1–10
5. Goldberg HI, Grossman RI, Gomori JM, Asbury AK, Bilaniuk LT, Zimmerman RA (1986) Cervical internal carotid artery dissecting hemorrhage: diagnosis using MR. Radiology 158(1):157–161
6. Rothrock JF, Lim V, Press G, Gosink B (1989) Serial magnetic resonance and carotid duplex examinations in the management of carotid dissection. Neurology 39(5):686–692
7. Naggara O, Louillet F, Touze E, Roy D, Leclerc X, Mas JL, Pruvo JP, Meder JF, Oppenheim C (2010) Added value of high-resolution MR imaging in the diagnosis of vertebral artery dissection. AJNR Am J Neuroradiol 31(9):1707–1712
8. Flis CM, Jager HR, Sidhu PS (2007) Carotid and vertebral artery dissections: clinical aspects, imaging features and endovascular treatment. Eur Radiol 17(3):820–834
9. Anzalone N, Cadioli M (2011) Vertebral artery dissection: looking for the ideal study protocol. AJNR Am J Neuroradiol 32(5):E91, author reply E92
10. Bachmann R, Nassenstein I, Kooijman H, Dittrich R, Kugel H, Niederstadt T, Kuhlenbaumer G, Ringelstein EB, Kramer S, Heindel W (2006) Spontaneous acute dissection of the internal carotid artery: high-resolution magnetic resonance imaging at 3.0 tesla with a dedicated surface coil. Investig Radiol 41(2):105–111
11. Ozdoba C, Sturzenegger M, Schroth G (1996) Internal carotid artery dissection: MR imaging features and clinical-radiologic correlation. Radiology 199(1):191–198
12. Stanisz GJ, Odrobina EE, Pun J, Escaravage M, Graham SJ, Bronskill MJ, Henkelman RM (2005) T1, T2 relaxation and magnetization transfer in tissue at 3T. Magn Reson Med 54(3):507–512
13. Busse RF, Brau AC, Vu A, Michelich CR, Bayram E, Kijowski R, Reeder SB, Rowley HA (2008) Effects of refocusing flip angle modulation and view ordering in 3D fast spin echo. Magn Reson Med 60(3):640–649
14. Bernstein MA, Fain SB, Riederer SJ (2001) Effect of windowing and zero-filled reconstruction of MRI data on spatial resolution and acquisition strategy. J Magn Reson Imaging 14(3):270–280
15. Landis JR, Koch GG (1977) The measurement of observer agreement for categorical data. Biometrics 33(1):159–174
16. Schievink WI (2001) Spontaneous dissection of the carotid and vertebral arteries. N Engl J Med 344(12):898–906
17. Habs M, Pfefferkorn T, Cyran CC, Grimm J, Rominger A, Hacker M, Opherk C, Reiser MF, Nikolaou K, Saam T (2011) Age determination of vessel wall hematoma in spontaneous cervical artery dissection: a multi-sequence 3T cardiovascular magnetic resonance study. J Cardiovasc Magn Reson 13:76
18. Cha JG, Jin W, Lee MH, Kim DH, Park JS, Shin WH, Yi BH (2011) Reducing metallic artifacts in postoperative spinal imaging: usefulness of IDEAL contrast-enhanced T1- and T2-weighted MR imaging—phantom and clinical studies. Radiology 259(3):885–893
19. Edjlali M, Roca P, Rabrait C, Naggara O, Oppenheim C (2012) 3D fast spin-echo T1 black-blood imaging for the diagnosis of cervical artery dissection. AJNR Am J Neuroradiol. doi: 10.3174/ajnr.A3261